Thermosensitive Core−Shell Particles as Carrier Systems for Metallic Nanoparticles

Yan Lu,* Yu Mei, and Matthias Ballauff*

Physikalische Chemie I, University of Bayreuth, 95440 Bayreuth, Germany

Markus Drechsler

Makromolekulare Chemie II, University of Bayreuth, 95440 Bayreuth, Germany

Received: December 8, 2005; In Final Form: January 23, 2006

We present a new system that allows us to modulate the catalytic activity of metal nanoparticles (Ag) by a thermodynamic transition that takes place within the carrier system. Thermosensitive core−shell particles have been used as the carrier system in which the core consists of poly(styrene) (PS), whereas the shell consists of a poly(*N*-isopropylacrylamide) (PNIPA) network cross-linked by *N*,*N*′-methylenebisacrylamide (BIS). Immersed in water, the shell of these particles is swollen. Heating the suspension above 32 °C leads to a volume transition within the shell that is followed by a marked shrinking of the network of the shell. The maximum degree of swelling can be adjusted by the degree of cross-linking. Silver nanoparticles with diameters ranging from 6.5 to 8.5 nm have been embedded into thermosensitive PNIPA networks with different cross-linking densities. The Ag nanoparticles do not influence the swelling and the shrinking of the network in the shell. The surface plasmon absorption band of the nanoparticles is shifted to higher wavelengths with temperature. This is traced back to the varying distance of the nanoparticles caused by the swelling and the shrinking of the shell. The catalytic activity is investigated by monitoring photometrically the reduction of 4-nitrophenol by an excess of $NaBH_4$ in the presence of the silver nanocomposite particles. The rate constant k_{app} was found to be strictly proportional to the total surface of the nanoparticles in the system. Moreover, k_{app} is first decreasing with increasing temperature when approaching the volume transition. This is due to the strong shrinking of the network. Only at temperatures above the volume transition is the normal Arrhenius-type dependence of k_{app} found again. In this way, catalytic activity of the metal nanoparticles enclosed in a "nanoreactor" can be modulated by volume transition over a wide range.

Introduction

In recent years, the immobilization of metal nanoparticles[1] in a polymeric matrix such as dendrimers,[2−4] latex particles,[5−12] microgels,[13−18] or other polymers[19−21] has fascinated scientists because of the importance such systems may have in nanotechnology. Metal nanoparticles exhibit size-induced quantum effects,[1,22] and have possible applications as sensors[23] and in electronics and catalysis.[24−27] More recently, Kumacheva and co-workers[17,18] introduced polymer microgels as carrier systems for nanoparticles. Thus, dendrimers or microgels may be viewed as "nanoreactors" in which metal nanoparticles can be immobilized and handled in an easier fashion.

In most cases studied so far, the polymer matrix provides only a suitable support for the metal nanoparticles and prevents them from aggregation. Recently, we have reported the first system that allows us to modulate the activity of nanoparticles by a thermodynamic transition that takes place within the carrier system.[28] The principle is shown in Figure 1: metallic nanoparticles are embedded in a polymeric network attached to a colloidal core particle. In all cases to be discussed here, the core consists of poly(styrene) (PS), whereas the network consists of poly(*N*-isopropylacrylamide) (PNIPA) cross-linked by *N*,*N*′-methylenebisacrylamide (BIS). The particles are suspended in water that swells the PNIPA at room temperature. The PNIPA network, however, undergoes a volume transition around 32 °C in which most of the water is expelled. Earlier experiments[29−31] have demonstrated that this transition is perfectly reversible. Hence, the process of shrinking and reswelling can be repeated without degradation or coagulation of the particles. With an increase in the amount of BIS in the system, the PNIPA network is more densely cross-linked and the degree of swelling and shrinking of the network becomes less pronounced.

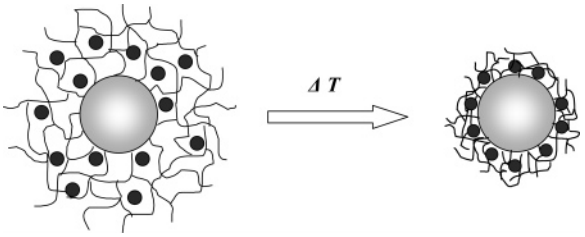

Figure 1. Schematic representation of PS-NIPA−Ag composite particles consisting of thermosensitive core−shell particles in which metallic nanoparticles (here, Ag) are embedded. The composite particles are suspended in water, which swells the thermosensitive network attached to the surface of the core particles. In this state, the reagents can diffuse freely to the nanoparticles that act as catalysts. At higher temperatures (T > 30 °C), the network shrinks and the catalytic activity of the nanoparticles is strongly diminished in this state.

Here, we investigate the optical properties, thermosensitivity, and catalytic activity of the composite particles in detail. In particular, the cross-linking density of the carrier system has

* E-mail addresses of the corresponding authors: yan.lu@uni-bayreuth.de (Y.L.); matthias.ballauff@uni-bayreuth.de (M.B.).

10.1021/jp057149n CCC: $33.50
Published on Web 02/14/2006

TABLE 1: Preparation of PS-NIPA Particles

sample	PS core[a] [g]	NIPA [g]	BIS [g]	KPS [g]	water [g]	R_h[b] [nm]
KPS1	347.67	40.07	1.37	0.40	500	127
KPS2	391.95	38.17	2.75	0.40	422.45	110
KPS3	416.82	39.99	5.46	0.40	449	101

[a] The solid content of the PS core dispersion is 10.51 wt %. [b] R_h was measured at 20 °C by DLS.

been changed in a systematic fashion. Moreover, the influence of the content of metal nanoparticle on the catalytic activity of the system is considered. Cryogenic transmission electron microscopy (cryo-TEM) is an effective method to investigate the morphology of a polymer in situ.[32,33] Recently, the morphology of spherical polyelectrolyte brushes and thermosensitive PS-NIPA core−shell particles have been successfully investigated by cryo-TEM.[34,35] In this paper, the morphology of the composite particles will be studied in detail by combining field-emission scanning electron microscopy (FESEM) and cryo-TEM.

As for the model reaction of catalysis, we chose the reduction of 4-nitrophenol, which is one of the most refractory pollutants that can occur in industrial wastewaters. The reduction of 4-nitrophenol to 4-aminophenol is of industrial importance as 4-aminophenol is a commercially important intermediate for the manufacture of analgesic and antipyretic drugs. Moreover, reduction of 4-nitrophenol is a very useful reaction for investigating catalytic activities because it has a strong absorption band at 400 nm at a high pH while the resulting 4-aminophenol is transparent. The reaction has been repeatedly used to check the catalytic activity of metal nanoparticles, and the results obtained in the present study can directly be compared to these reports.[25,36,37] We shall demonstrate that the properties of the nanoreactor can be tuned over a wide range by the cross-linking density of the shell.

Experimental Part

Materials. *N*-isopropylacrylamide (NIPA; Aldrich), *N*,*N*′-methylenebisacrylamide (BIS; Fluka), sodium dodecyl sulfate (SDS; Fluka), and potassium peroxodisulfate (KPS; Fluka) were used as received. Styrene (BASF) was destabilized by an Al_2O_3 column and stored in the refrigerate. Silver nitrate ($AgNO_3$; Aldrich) and reducing agent sodium borohydride ($NaBH_4$; Aldrich) were used as commercially available. 4-Nitrophenol was obtained from Aldrich and used as received.

The core−shell type PS-NIPA particles were synthesized and characterized as described recently.[38−43] In the first step, PS core latex was prepared by conventional emulsion polymerization using styrene (253.2 g) and NIPA (13.75 g) as monomers, SDS (2.34 g dissolved in 925 g of water) as the surfactant, and KPS (0.50 g dissolved in 20 g of water) as the initiator. The reaction was run at 80 °C for 8 h. Purification was done by ultrafiltration with 10 times volume of water. In the second step, the PS-NIPA core−shell system was prepared by seeded emulsion polymerization. Table 1 summarizes the amounts of ingredients used for preparation of the PS-NIPA particles.

The preparation of silver nanoparticles in an aqueous solution was carried out by the chemical reduction of the metal salt−PS-NIPA mixture with sodium borohydride. For a typical experiment, 0.575 mL of a $AgNO_3$ (0.1 M) solution was added to a PS-NIPA aqueous solution (2 g PS-NIPA latex diluted with 98 g of water), and the mixture was stirred for 30 min under N_2. Thereafter, sodium borohydride (0.043 g dissolved in 5 g of water) was quickly added to the solution under stirring for 1 h. Finally, the silver nanocomposite particles were cleaned by serum replacement against purified water (membrane: cellulose nitrate with a 100 nm pore size supplied by Schleicher & Schuell).

Catalytic Reduction of 4-Nitrophenol. In this study, first 0.5 mL of sodium borohydride (1.2 mg) was added to 2.5 mL of 4-nitrophenol (0.042 mg) contained in a glass vessel. After that, a given amount of silver nanoparticles was added to it. Immediately after addition of metal nanoparticles, UV spectra of the sample were taken every 30 s in the range of 250−550 nm. The rate constant of the reaction was determined by measuring the change in intensity of the initially observed peak at 400 nm with time.

Characterization of PS-NIPA−Ag Composite Particles. Cryogenic transmission electron microscopy (cryo-TEM) specimens were prepared by vitrification of thin liquid films supported on a TEM copper grid (600 mesh, Science Services, Munich, Germany) in liquid ethane at its freezing point. The specimen was inserted into a cryotransfer holder (CT3500, Gatan, Munich, Germany) and transferred to a Zeiss EM922 EFTEM (Zeiss NTS GmbH, Oberkochen, Germany). Examinations were carried out at temperatures around 90 K. The TEM was operated at an acceleration voltage of 200 kV. All images were recorded digitally by a bottom-mounted CCD camera system (UltraScan 1000, Gatan, Munich, Germany) and were processed with a digital imaging processing system (Digital Micrograph 3.9 for GMS 1.4, Gatan, Munich, Germany).[34]

Field-emission scanning electron microscopy (FESEM) was performed using a LEO Gemini microscope equipped with a field emission cathode. Dynamic light scattering (DLS) measurements were done using an ALV 4000 light scattering goniometer (Peters) at different temperatures and a scattering angle of 90°. The UV spectra were measured by a Lambda 25 spectrometer supplied by Perkin-Elmer. The silver content was determined by thermogravimetric analysis (TGA) using a Mettler Toledo STARe system. After drying in the vacuum overnight, the silver composites were heated to 800 °C with a heating rate of 10 °C/min under N_2. TGA measurements for the polymeric templates show that the polymeric network will be completely decomposed when the temperature is up to 500 °C. This indicates that the substance left at 800 °C in the composite system can be attributed to the pure silver content. The theoretical specific surface area of silver particles was estimated from these TGA results, and the particle size was estimated from cryo-TEM. For this calculation, the density of bulk silver was used ($\rho = 10.5$ g/cm^3).

Results and Discussion

PS-NIPA−Ag Nanocomposites. Figure 2 shows the SEM images for the PS-NIPA particles and silver composite particles. From Figure 2, it can be observed clearly that some bright dots are seen on the surface of the PNIPA shell of the monodispersed PS-PNIPA carrier particles. However, micrographs taken by field-emission electron microscopy (FESEM) refer to the dried state in which the PNIPA network is totally shrunken. To study the morphology of silver composite particles in situ, that is, in the swollen state, cryogenic transmission electron microscopy (cryo-TEM) has to be used. Figure 3 displays the cryogenic transmission electron microscopy (cryo-TEM) images of PS-NIPA−Ag particles prepared by PNIPA networks with different cross-linking densities. In Figure 3, the dark spherical area indicates the PS core, whereas the light corona around the dark core is the PNIPA shell of the particle. The particle size distribution histograms of Ag nanoparticles evaluated from corresponding cryo-TEM images are shown in Figure 4. The

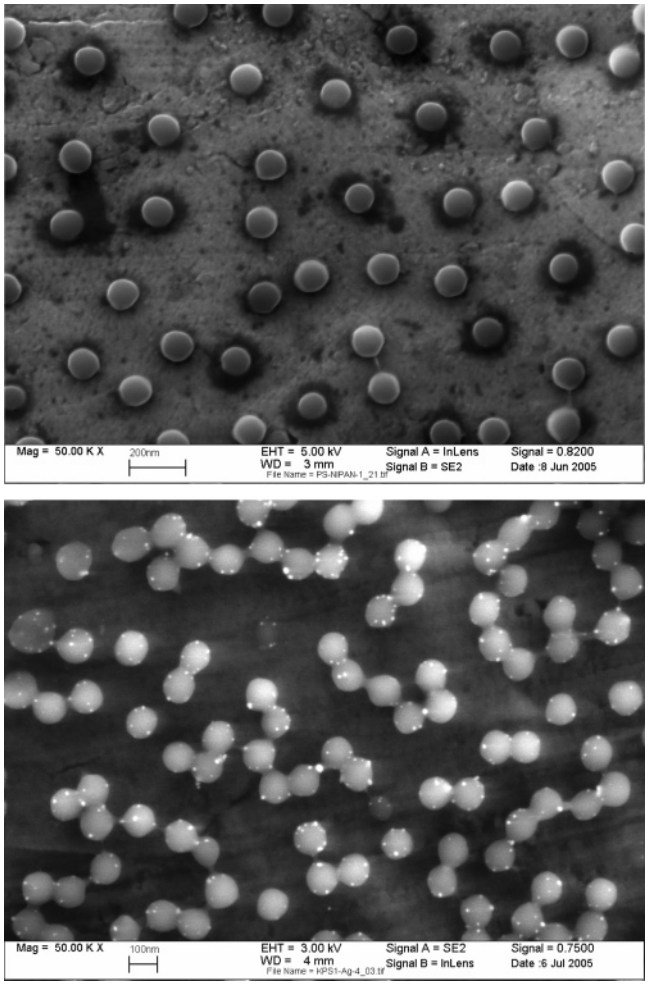

Figure 2. FESEM images for PS-NIPA carrier particles (KPS1, 2.5 mol % BIS) (top) and PS-NIPA−Ag composite particles (KPS1−Ag) (bottom).

Ag nanoparticles are seen as the small black dots. Comparing the cryo-TEM images with the micrographs obtained by FESEM, it is evident that most of the silver nanoparticles are immobilized inside the PNIPA networks affixed to the surface of the core particles. This is the case for all cross-linking densities under consideration.

The immobilization of Ag nanoparticles may be due to the strong localization of the Ag^+ ions within the network which is most probably caused by a complexation of the Ag^+ ions by the nitrogen atoms of the PNIPA.[44] Thermogravimetric analysis measurements indicate that 10.4, 10.2, and 10.3 wt % Ag had been embedded into the KPS1, KPS2, and KPS3 carrier systems, respectively. Furthermore, the decrease of the corona size with an increase in the amount of BIS corresponds to the increase of the cross-linking density in the carrier system. It is also interesting to note that Ag nanoparticles are located mostly at the edge of the corona instead of near the dark PS core when Ag nanocomposites are prepared by higher cross-linked PS-NIPA particles. In case of higher cross-linking densities, smaller Ag particles are generated in the system. This becomes obvious when comparing the size of the particles for the different systems (cf. Table 1): When 2.5, 5, and 10 mol % BIS is used for cross-linking, the size of Ag nanoparticles is given by 8.5 (±1.5), 7.3 (±1.5), and 6.5 nm (±1.0 nm), respectively. This could be due to the possible limitation of the growth of Ag nanoparticles in the densely cross-linked network. Moreover, since the amount of Ag embedded into the network is the same, smaller but more Ag nanoparticles are generated with the increase of the cross-linking density.

Figure 5 shows the hydrodynamic radii of the carrier particles (top) and the composite particles (bottom). Dynamic light scattering measurements of composite particles at different temperatures indicate that the thermosensitivity of the PNIPA network, that is, its shrinking and reswelling, is not hampered by the incorporation of metal nanoparticles into the network. The Ag−composite particles show a similar volume transition temperature as the carrier particle at 32 °C which is in excellent agreement with previous findings on these systems.[38−41] This indicates that metal nanoparticles do not disturb the volume transition within the network. Moreover, with the increase of the cross-linker content in the system, the transition temperature of the carrier systems remains constant. However, the degree of shrinking of the network with temperature is decreasing as is expected for a network with a higher cross-linking density.

Figure 6 shows representative UV spectra of the PS-NIPA−$AgNO_3$ aqueous solution before and after reduction with sodium borohydride. The absorption spectra display a significant plasmon band after the addition of sodium borohydride. This absorption is characteristic of metallic silver colloids.[22,45] It can be seen that the surface plasmon absorption band of the PS-NIPA−Ag composites is rather sharp and peaks at 401 nm. This agrees with the results of Kumacheva and co-workers[17] who obtained similar values for silver nanoparticles in the interior of microgels. It indicates that Ag nanoparticles with a narrow size distribution have been formed in these systems.

UV spectra have also been recorded for diluted silver nanocomposites at different temperatures. UV spectra of a PS-NIPA dispersion with a similar concentration were measured at the same temperature as the reference sample. To obtain the signal of the Ag nanoparticles, this reference was subtracted from the spectra of the composite particles. Figure 7 shows the resulting net spectra of the Ag particles. Figure 8 shows the shift of the plasmon peak with temperature correlating to the volume transition of the network. The plasmon peak of the silver nanocomposites is originally centered at ∼400 nm at lower temperatures, and an obvious red shift of the plasmon peak to ∼410 nm can be observed when the temperature is higher than 30 °C. The shift to longer wavelengths and broadening of the surface plasmon absorption band can thus be induced by the volume transition of thermosensitive PNIPA networks. It should be noted that this transition is fully reversible upon cooling to room temperature.

At lower temperatures, Ag nanoparticles are rather widely separated within the mesh of the PNIPA network. Cryo-TEM images indicate that the distance between Ag nanoparticles is around 30−40 nm when they are in the swollen state, which is too large to cause the red shift of the absorption. Hence, no obvious red shift of the maxima of the plasmon peak can be found for the system when we increase the temperature from 10 to 20 °C. However, when the temperature is up to 30 °C, the network shrinks markedly (see Figures 5 and 8) and the average distance of the embedded Ag nanoparticles must decrease significantly. In this case, a shift of the surface plasmon absorption band to longer wavelengths can be investigated. From Figure 8, it can be seen clearly that the shift of the plasmon peak of Ag nanoparticles with increasing temperature correlates with the reciprocal hydrodynamic radius. Hence, we assign the shift of the maxima to the varying distance between the nanoparticles brought about by the shrinking and reswelling of the network. The full reversibility indicates, however, that the

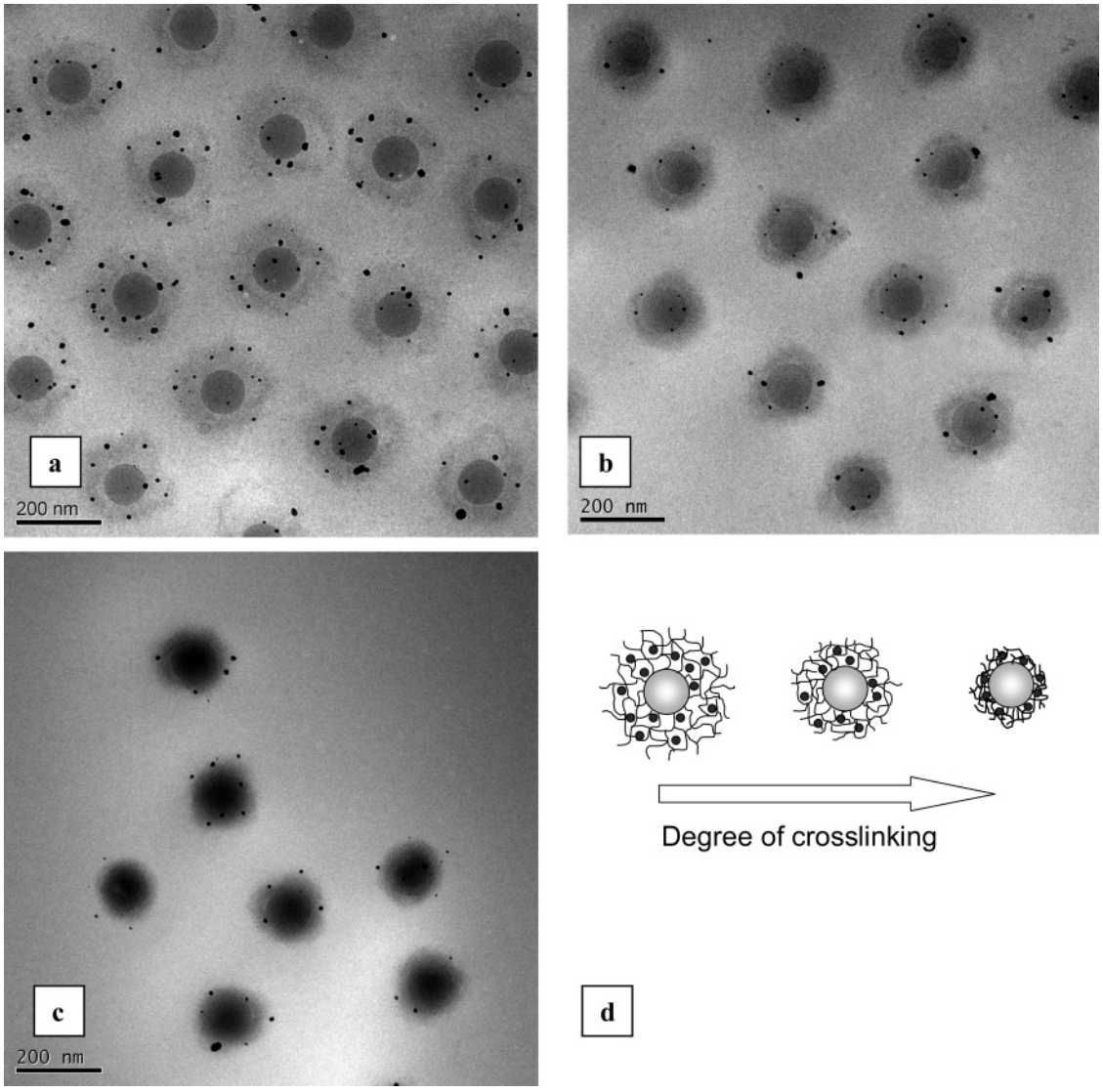

Figure 3. Cryo-TEM images for the silver nanocomposite particles prepared by PS-NIPA particles with different cross-linker content: (a) KPS1−Ag, 2.5 mol % BIS; (b) KPS2−Ag, 5 mol % BIS; (c) KPS3−Ag, 10 mol % BIS; (d) schematic representation of the influence of the degree of cross-linking on the morphology of silver composite particles.

particles are still kept separately and no coagulation takes place within the network.

Catalytic Reduction of 4-Nitrophenol. The kinetics of 4-nitrophenol reduction in the presence of metal nanocomposite particles was studied by UV/VIS spectroscopy. Since the concentration of metal−composite particles in the system is very low (ca. 6 mg/L), the absorption spectra of 4-nitrophenol will not be disturbed by the light scattering of the carrier particles. Figure 9 shows the UV spectra for the reduction of 4-nitrophenol measured at different times. For a typical measurement, a successive decrease of peak intensity at 400 nm with time can be used to obtain the rate constant.[28,37,46] This peak is attributed to the presence of 4-nitrophenate ions in the system. The formation of 4-nitrophenate ions takes place immediately after addition of $NaBH_4$ to the system. After addition of Ag nanocomposite particles, it was found that the peak height at 400 nm gradually decreases with time. With a gradual decrease in peak height at 400 nm, a new peak is appearing at 290 nm. Moreover, two points can be observed in the UV spectra where all spectra intersect each other. This indicates that in the catalytic reduction reaction the conversion of 4-nitrophenol gives only one product, namely 4-aminophenol.[36] The conversion of the process can be directly read off these curves as the ratio of the concentration c_t of the 4-nitrophenol at time t to its value c_0 at $t = 0$ is directly given by the ratio of the respective absorbances A/A_0. Since the concentration of sodium borohydride largely exceeds the concentration of 4-nitrophenol, the reduction rates can be assumed to be independent of borohydride concentration. So, in this case, a first-order rate kinetics with regard to the 4-nitrophenol concentrations could be used to evaluate the catalytic rate.[3,47] Moreover, the apparent rate constant k_{app} will certainly be proportional to the surface S of the metal nanoparticles present in the system:[37]

$$-\frac{dc_t}{dt} = k_{app}c_t = k_1 S c_t \quad (1)$$

where c_t is the concentration of 4-nitrophenol at time t and k_1 is the rate constant normalized to S, the surface area of Ag nanoparticles normalized to the unit volume of the system.

As shown by Figure 10, linear relations between $\ln(c_t/c_0)$ versus time t have been obtained in all cases. Here, attention must be paid to the fact that a delay time t_0 was found for the catalytic reduction, which may be due to an activation of the catalyst in the reaction mixtures. This is in accord with other studies of the catalysis of this reaction by metal nanopar-

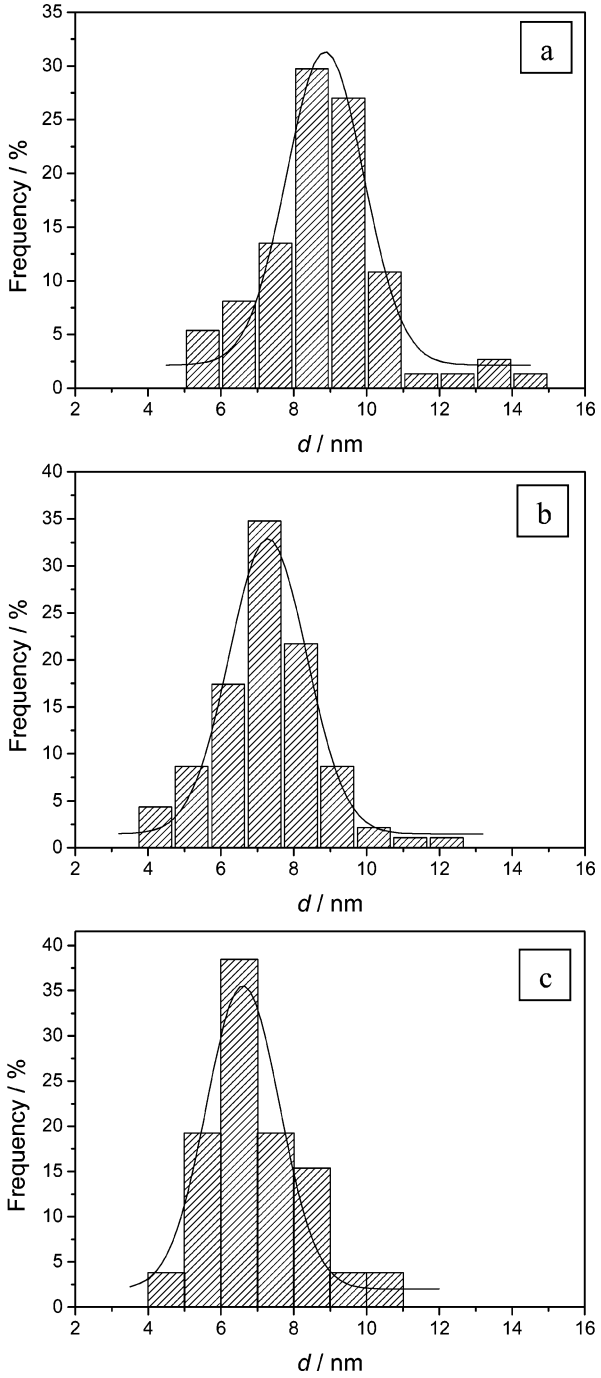

Figure 4. Particle size distribution histograms of silver composite particles evaluated from the corresponding cryo-TEM images shown in Figure 3: (a) KPS1−Ag, 2.5 mol % BIS; (b) KPS2−Ag, 5 mol % BIS; (c) KPS3−Ag, 10 mol % BIS. The solid lines are Gaussian fits of the data.

ticles.[3,25,36,37] Also, the induction period observed at the initial stages of reaction becomes shorter if the silver concentration increases in the system.

Figure 11 shows the values of the apparent rate constant k_{app} measured both at 20 and 40 °C as a function of the concentration of Ag−composite particles and the theoretical specific surface area of Ag particles, respectively. For the calculation of the surface area of Ag nanoparticles, the bulk density of silver was used ($\rho = 10.5$ g/cm^3). TGA and cryo-TEM results have been used to estimate the number and size of silver particles, respectively. From Figure 11a, it can be observed that the increase of the concentration of the silver nanoparticles in the

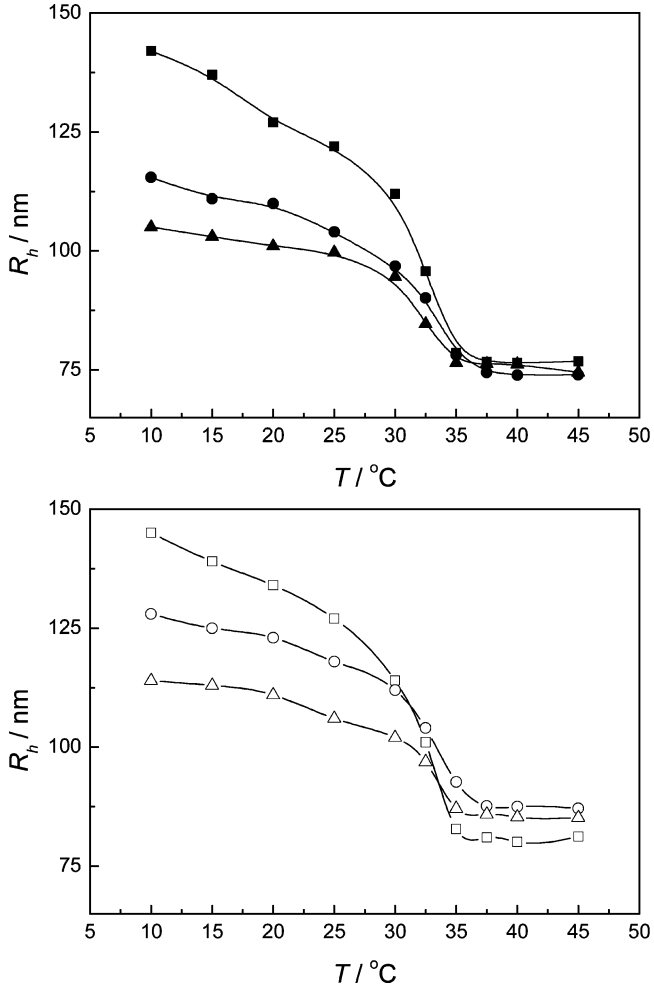

Figure 5. Hydrodynamic radii vs temperature for PS-NIPA particles (top): (filled square) KPS1, 2.5 mol % BIS; (filled circle) KPS2, 5 mol % BIS; (filled triangle) KPS3, 10mol % BIS. Hydrodynamic radii vs temperature for PS-NIPA−metal composite particles (bottom): (open square) KPS1−Ag; (open circle) KPS2−Ag; (open triangle) KPS3−Ag.

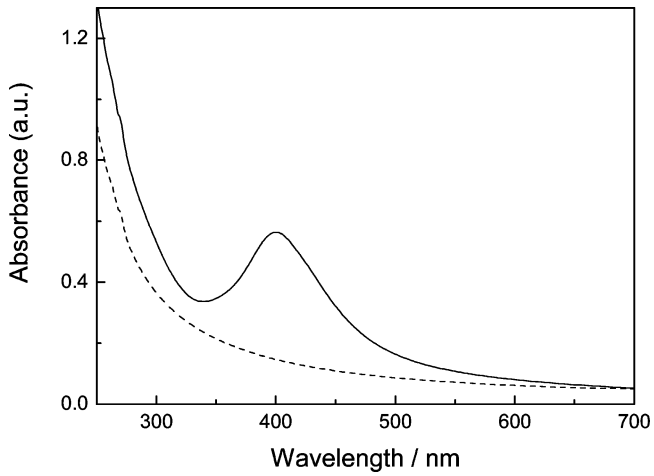

Figure 6. UV spectra of PS-NIPA−$AgNO_3$ solution before (dashed line) and after (solid line) reduction.

system leads to a rapid increase of the rate constant. This is found for all cross-linking densities or temperatures. This is to be expected from eq 1 and has been found for other systems as well.[37]

There is a strict relation between k_{app} and the surface of the silver nanoparticles as will be shown in the following: As

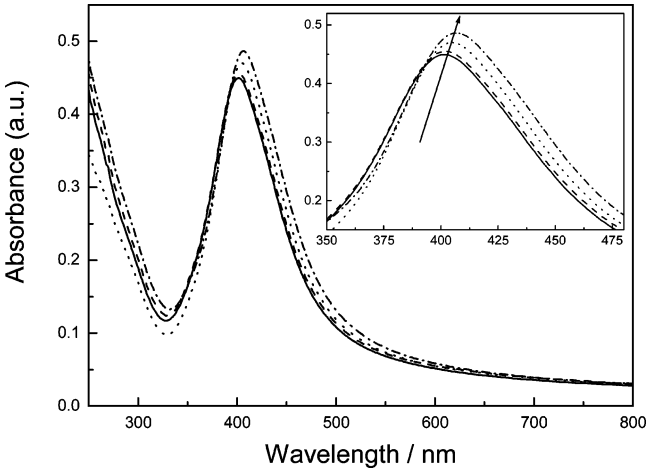

Figure 7. UV spectra of PS-NIPA−Ag nanocomposites measured at different temperatures: (solid line) at 10 °C; (dashed line) at 20 °C; (dotted line) at 30 °C; (dashed−dotted line) at 40 °C.

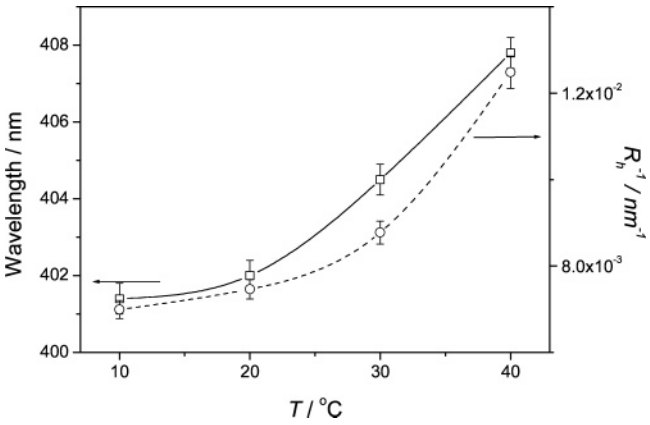

Figure 8. Maxima of plasmon peak (open square) and the reciprocal hydrodynamic radius (open circle) vs temperature for KPS1−Ag nanocomposites. The good correlation between the two sets of data indicates that the red shift of the plasmon peak is related to the average distance between the particles.

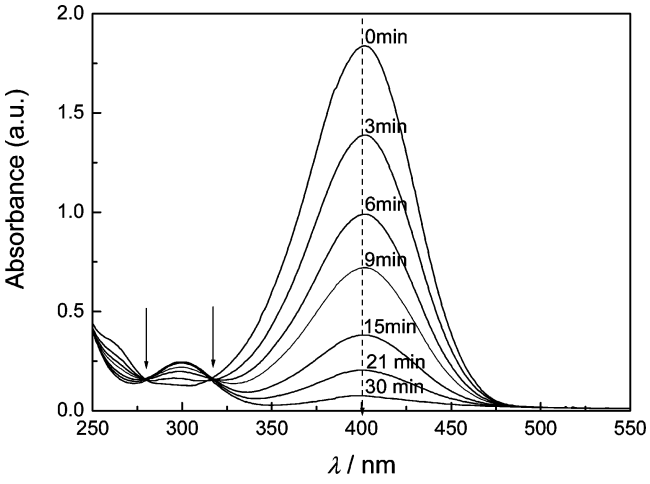

Figure 9. UV spectra of solutions of 4-nitrophenol measured at different times *t* indicated in the graph. The arrows mark the points where all spectra intersect each other.

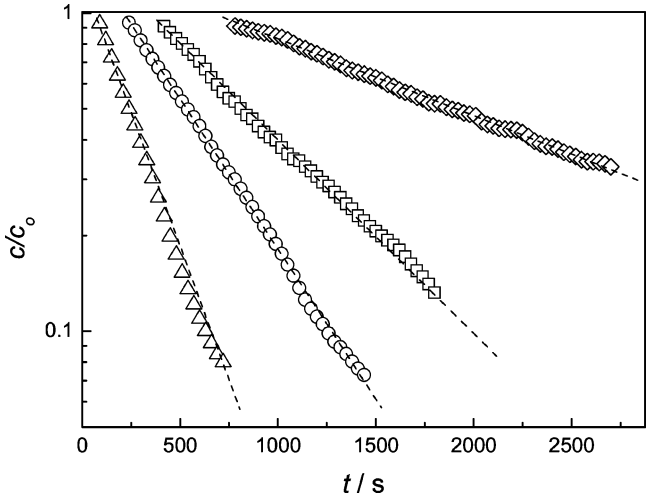

Figure 10. Influence of Ag−composite particles (KPS2−Ag) concentration on the reduction of 4-nitrophenol. The concentration of the reactants was as follows: [4-nitrophenol] = 0.1 mmol/L, [$NaBH_4$] = 10 mmol/L, T = 20 °C. The variable of the different curves is the concentration of composite particles in the solution: (diamonds) 2.28 mg/L; (squares) 4.56 mg/L; (circles) 6.94 mg/L; (triangles) 11.4 mg/L.

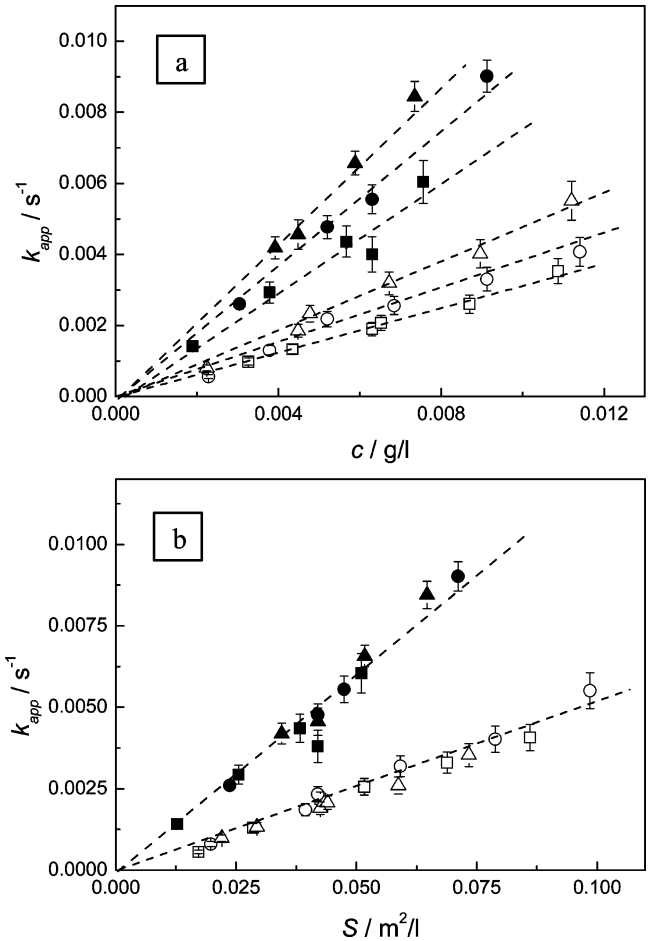

Figure 11. (a) Rate constant k_{app} as a function of the concentration of Ag−composite particles. (b) Rate constant k_{app} as a function of the surface area S of Ag nanoparticles normalized to the unit volume of the system: (squares) KPS1−Ag; (circles) KPS2−Ag; (triangles) KPS3−Ag; (filled symbols) T = 40 °C; (open symbols) T = 20 °C; [4-nitrophenol] = 0.1 mmol/L, [$NaBH_4$] = 10 mmol/L.

already discussed above, an increase of the cross-linking density leads to smaller silver nanoparticles. Since the same amount of Ag has been immobilized in every system, a greater number of smaller particles is therefore formed when the cross-linking density is higher. This, in turn, increases the total surface area of the silver particles in the system. Figure 11a has shown that k_{app} varies in a strictly linear fashion with the concentration of

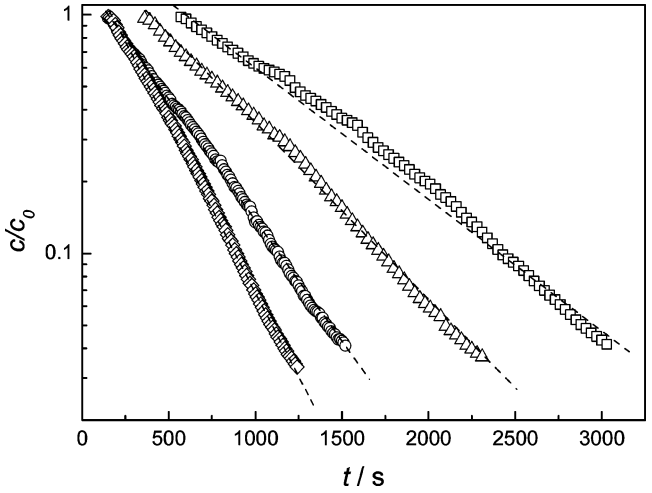

Figure 12. Influence of temperature on the kinetic constant k measured with PS-NIPA−Ag system KPS3−Ag (see Table 1). The variable of the different curves is the temperature T. (squares) 283 K; (triangles) 288 K; (circles) 303 K, (diamonds) 308 K. The concentrations are follows: [KPS3−Ag] = 4.5×10^{-3} g/L, [4-nitrophenol] = 0.1 mmol/L, [$NaBH_4$] = 10 mmol/L.

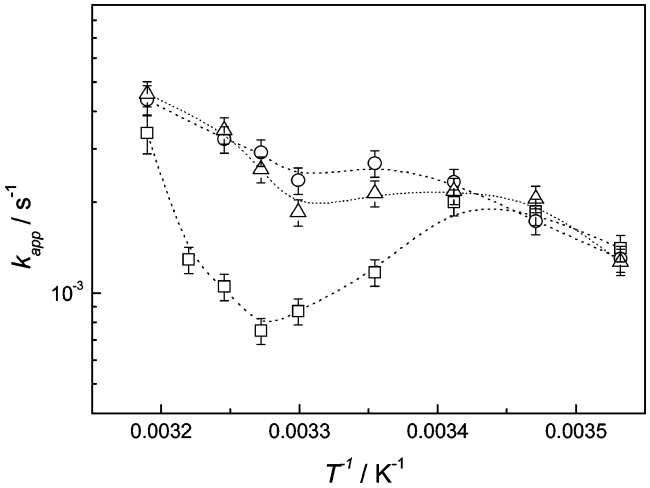

Figure 13. Arrhenius plot of the reaction rate $k(T)$ measured in the presence of PS-NIPA−Ag composite particles at different temperatures: (squares) KPS1−Ag, 2.5 mol % BIS; (triangles) KPS2−Ag, 5 mol % BIS; (circles) KPS3−Ag, 10 mol % BIS. The concentrations of the reactants are as follows: (composite particles) $S = 0.042$ m^2/L; [4-nitrophenol] = 0.1 mmol/L, [$NaBH_4$] = 10 mmol/L. The broken lines are guidelines for the eye.

catalytic particles. However, the slopes of these curves have been found to increase with increasing cross-linking density. However, reducing k_{app} to the specific surface area of catalytic particles S leads to a master curve for all systems again. This is shown in Figure 11b which validates the assumption given in eq 1. Hence, the catalysis takes place on the surface of the nanoparticles and the catalytic activity at a given temperature must, hence, depend on the total surface area S of the silver nanoparticles immobilized per unit volume of the carrier suspension. The same is found for 40 °C, that is, for temperatures far above the volume transition.

As reported by Pradhan et al.,[36] Ag nanoparticles with an average size of ~25 nm have been used as the catalyst in the reduction of 4-nitrophenol by sodium borohydride. They obtained a rate constant of $k_{app} = 2.3 \times 10^{-3}$ s^{-1} with 5×10^{-6} mol/L Ag catalyst at 20 °C. Normalizing the rate constant to the surface of the particles in the system, they got $k_1 = 3.78 \times 10^{-7}$ L s^{-1} m^{-2}. In our system, the size of Ag nanoparticles is much smaller in all cases. From Figure 11b, $k_1 = 5.2 \times 10^{-2}$ L s^{-1} m^{-2} can be calculated for the PS-NIPA−Ag composite particles. This demonstrated that the smaller particles used in the present study exhibit a significantly higher activity, which indicates that the specific turnover frequencies (TOFs) based upon the Ag particle surface areas are much higher.

We now turn to the influences of the temperature on k_{app}. Figure 12 shows the experimental data referring to temperatures ranging from 10 to 40 °C. Again, pseudo-first-order kinetics is seen at all temperatures T. Moreover, the delay time t_0 is reduced with increasing temperature as expected from the analysis of other systems.[37] The rate constants $k_{app}(T)$ obtained from PS-PNIPA−Ag composite particles from this analysis are shown in Figure 13. The variable in this figure is the different cross-linking densities of the shells of the particles. Figure 13 demonstrates that the rate constants k_{app} obtained at different temperatures do not follow the typical Arrhenius-type dependence on temperature. In the PS-NIPA−Ag system, there are two factors influencing the rate constants k_{app} with temperature: one is the diffusional barrier caused by the shrinkage of the network with temperature,[29−31] which will slow the diffusion of reactant, thus decreasing the rate constant; another is thermoactivity, which will increase the rate constant with temperature. From Figure 13, it can be seen that the change of k_{app} with temperature can be divided into three regions, which is due to the volume transition of PNIPA network: When the reaction temperature is lower than room temperature, the PNIPA networks with different cross-linking densities are all in the totally swollen state in water. In this case, Ag nanoparticles, which have been embedded in the network, can be fully accessed by the reactants of the catalytic reduction. So, the rate constant k_{app} will exhibit a simple linear relation of ln k_{app} with T^{-1}. However, when the temperature is further increasing, the PNIPA network shrinks markedly, which is followed by a concomitant slowing of the diffusion of reactants within the network. This, in turn, will lower the rate of the reaction catalyzed by the silver nanoparticles. It is obvious that the increase of k_{app} caused by raising the temperature is now overcome by the diffusional barrier. Hence, the reaction rate must reach its minimum at the transition temperature. If the increase of temperature continues, the PNIPA network will not shrink any more and the density within the network will stay constant. Now, the strong increase of k_{app} with T will be predominant and the reaction rate will rise again.

As shown in Figure 13, the rate constant k_{app} with temperature reaches a minimum in all three systems. However, with the increase of the cross-linking density in the system, this minimum is less pronounced. This can be explained as follows: The shrinking of the PNIPA network becomes smaller (see Figure 5). In this case, for the highly cross-linked system, the influence of the diffusional barrier caused by raising the temperature on the rate constant will be not so strong as that for systems with lower cross-linking densities. In the limiting case of a high cross-linking density, the shrinking of the network in the shell of the particles will become marginal. In this case, the composite particles will exhibit the conventional Arrhenius behavior of k_{app}.

Conclusions

Thermosensitive PNIPA networks with different cross-linking densities can be used as carrier system for silver nanoparticles. The optical property of PS-NIPA−Ag composites is influenced by the volume transition of the PNIPA network and exhibits a shift of the surface plasmon absorption band of the Ag

nanoparticles with temperature. The PS-NIPA−Ag composites can be used as catalysts for reduction reactions in the aqueous phase. We demonstrated that the catalytic activity of the Ag nanoparticles immobilized within the carrier particles can be modulated over 1 order of magnitude. In this way, the thermosensitive core−shell particles present a novel carrier system which can be used as a nanoreactor that can be opened and closed again to a certain extent.

Acknowledgment. The authors thank the Deutsche Forschungsgemeinschaft, SFB 481, Bayreuth, the BASF-AG, and Fonds der Chemischen Industrie for financial support.

References and Notes

(1) Burda, C.; Chen, X.; Narayanan, R.; El-Sayed, M. A. *Chem. Rev.* **2005**, *105*, 1025.
(2) Scott, R. W. J.; Wilson, O. M.; Crooks, R. M. *J. Phys. Chem. B* **2005**, *109*, 692 and references therein.
(3) Esumi, K.; Isono, R.; Yoshimura, T. *Langmuir* **2004**, *20*, 237.
(4) Liu, Z.; Wang, X.; Wu, H.; Li, C. *J. Colloid Interface Sci.* **2005**, *287* (2), 604.
(5) Siiman, O.; Burshteyn, A. *J. Phys. Chem. B* **2000**, *104*, 9795.
(6) Chen, C.; Chen, M.; Serizawa, T.; Akashi, M. *Adv. Mater.* **1998**, *10*, 1122.
(7) Kim, J.; Lee, J.; Ryu, J.; Lee, J.; Kim, S.; Han, S.; Chang, I.; Kang, H.; Suh, K. *J. Polym. Sci., Part A: Polym. Chem.* **2004**, *42*, 2551.
(8) Chen, C. W.; Serizawa, T.; Akashi, M. *Langmuir* **1999**, *15*, 7998.
(9) Sun, Q.; Deng, Y. *Langmuir* **2005**, *21*, 5812.
(10) Carotenuto, G. *Appl. Organomet. Chem.* **2001**, *15*, 344.
(11) Garotenuto, G.; Pepe, G. P.; Nicolais, L. *Eur. Phys. J. B* **2000**, *16*, 11.
(12) Velikov, K. P.; Zegers, G. E.; Blaaderen, A. *Langmuir* **2003**, *19*, 1384.
(13) Vincent, T.; Guibal, E. *Langmuir* **2003**, *19*, 8475.
(14) Biffis, A.; Orlandi, N.; Corain, B. *Adv. Mater.* **2003**, *15*, 1551.
(15) Biffis, A.; Sperotto, E. *Langmuir* **2003**, *19*, 9548.
(16) Pich, A.; Hain, J.; Lu, Y.; Boyko, V.; Prots, Y.; Adler, H.-J. *Macromolecules* **2005**, *38*, 6610.
(17) Zhang, J.; Xu, S.; Kumacheva, E. *J. Am. Chem. Soc.* **2004**, *126*, 7908.
(18) Zhang, J.; Xu, S.; Kumacheva, E. *Adv. Mater.* **2005**, *17*, 2336.
(19) Suzuki, D.; Kawaguchi, H. *Langmuir* **2005**, *21*, 8175.
(20) Mbhele, Z. H.; Salemane, M. G.; van Sittert, C. G. C. E.; Nedeljkovic, J. M.; Djolovic, V.; Luyt, A. S. *Chem. Mater.* **2003**, *15*, 5019.
(21) Sharma, G.; Ballauff, M. *Macromol. Rapid Commun.* **2004**, *25*, 547.
(22) Kamat, P. V. *J. Phys. Chem. B* **2002**, *106*, 7729.
(23) Frederix, F.; Friedt, J.; Choi, K.; Laureyn, W.; Campitelli, A.; Mondelaers, D.; Maes, G.; Borghs, G. *Anal. Chem.* **2003**, *75*, 6894.
(24) Jiang, Z.; Liu, C.; Sun, L. *J. Phys. Chem. B* **2005**, *109*, 1730.
(25) Praharaj, S.; Nath, S.; Ghosh, S.; Kundu, S.; Pal, T. *Langmuir* **2004**, *20*, 9889.
(26) Narayanan, R.; El-Sayed, M. A. *J. Phys. Chem. B* **2005**, *109*, 12663.
(27) Campbell, C. T.; Parker, S. C.; Starr, D. E. *Science* **2002**, *298*, 811.
(28) Lu, Y.; Mei, Y.; Drechsler, M.; Ballauff, M. *Angew. Chem., Int. Ed. Engl.* **2006**, *45*, 813.
(29) Dingenouts, N.; Norhausen, Ch.; Ballauff, M. *Macromolecules* **1998**, *31*, 8912.
(30) Kim, J.-H.; Ballauff, M. *Colloid Polym. Sci.* **1999**, *277*, 1210.
(31) Ballauff, M. *Macromol. Chem. Phys.* **2003**, *204*, 220.
(32) Nizri, G.; Magdassi, S.; Schmidt, J.; Talmon, Y. *Langmuir* **2004**, *20*, 4380.
(33) Li, Z.; Kesselman, E.; Talmon, Y.; Hillmyer, M. A.; Lodge, T. P. *Science* **2004**, *306*, 98.
(34) Wittemann, A.; Drechsler, M.; Talmon, Y.; Ballauff, M. *J. Am. Chem. Soc.* **2005**, *127*, 9688.
(35) Crassous, J.; Drechsler, Y.; Talmon, Y.; Ballauff, M. *Langmuir*, in press.
(36) Pradhan, N.; Pal, A.; Pal, T. *Colloids Surf., A* **2002**, *196*, 247.
(37) Mei, Y.; Sharma, G.; Lu, Y.; Drechsler, M.; Ballauff, M.; Irrgang, T.; Kempe, R. *Langmuir* **2005**, *21*, 12229.
(38) Dingenouts, N.; Ballauff, M. *Acta Polym.* **1998**, *49*, 178.
(39) Seelenmeyer, S.; Deike, I.; Dingenouts, N.; Rosenfeldt, S.; Norhausen, Ch.; Ballauff, M.; Narayanan, T. *J. Appl. Crystallogr.* **2000**, *33*, 574.
(40) Dingenouts, N.; Seelenmeyer, S.; Deike, I.; Rosenfeldt, S.; Ballauff, M.; Lindner, P.; Narayanan, T. *Phys. Chem. Chem. Phys.* **2001**, *3*, 1169.
(41) Seelenmeyer, S.; Deike, I.; Rosenfeldt, S.; Norhausen, Ch.; Ballauff, M.; Narayanan, T. *J. Chem. Phys.* **2001**, *114*, 10471.
(42) Duracher, D.; Sauzedde, F.; Elaissari, A.; Perri, A.; Pichot, C. *Colloid Polym. Sci.* **1998**, *276*, 219.
(43) Duracher, D.; Sauzedde, F.; Elaissari, A.; Pichot, C.; Nabzar, L. *Colloid Polym. Sci.* **1998**, *276*, 920.
(44) Frattini, A.; Pellegri, N.; Nicastro, D.; de Sanctis, O. *Mater. Chem. Phys.* **2005**, *94*, 148.
(45) Behrens, S.; Wu, J.; Habicht, W.; Unger, E. *Chem. Mater.* **2004**, *16*, 3085.
(46) Antipov, A. A.; Sukhorukov, G. B.; Fedutik, Y. A.; Hartmann, J.; Giersig, M.; Moehwald, H. *Langmuir* **2002**, *18*, 6687.
(47) Ghosh, S. K.; Mandal, M.; Kundu, S.; Nath, S.; Pal, T. *Appl. Catal. A* **2004**, *268*, 61.